DIRECT MEASUREMENTS OF ENERGETIC NEUTRAL HYDROGEN IN THE INTERPLANETARY MEDIUM

A. GALLI AND P. WURZ
University of Bern, Physikalisches Institut, CH-3012 Bern, Switzerland; galli@phim.unibe.ch

S. BARABASH, A. GRIGORIEV, R. LUNDIN, Y. FUTAANA, H. GUNELL, AND M. HOLMSTRÖM
Swedish Institute of Space Physics, Box 812, SE-981 28 Kiruna, Sweden

E. C. ROELOF
Applied Physics Laboratory, Johns Hopkins University, Laurel, MD 20723-6099

C. C. CURTIS AND K. C. HSIEH
University of Arizona, Tucson, AZ 85721

A. FEDOROV
Centre d'Etude Spatiale des Rayonnements, BP-4346, F-31028 Toulouse, France

D. WINNINGHAM AND R. A. FRAHM
Southwest Research Institute, San Antonio, TX 7228-0510

R. CERULLI-IRELLI
Instituto di Fisica dello Spazio Interplanetario, I-00133 Rome, Italy

P. BOCHSLER
University of Bern, Physikalisches Institut, CH-3012 Bern, Switzerland

AND

N. KRUPP, J. WOCH, AND M. FRAENZ
Max-Planck Institut für Aeronomie, D-37191 Katlenburg-Lindau, Germany

ABSTRACT

We present an analysis of hydrogen energetic neutral atoms (ENAs) measured by the ASPERA-3 instrument on board *Mars Express*. We focus on ENAs that have no Martian origin. The energy spectra of these ENAs are all very similar and can be fitted well by a two-component power law. The fluxes, integrated from 0.2 to 10 keV, vary between 5×10^3 and 10^5 cm^{-2} sr^{-1} s^{-1}. We checked for possible sources for these ENAs, but we can rule out a planetary origin, a solar wind origin, contamination by UV from UV bright stars, and contamination by high-energy protons. With our present knowledge we conclude that the heliospheric termination shock is the most plausible source region.

Subject headings: acceleration of particles — instrumentation: detectors — interplanetary medium — methods: data analysis — plasmas — solar wind

1. INTRODUCTION

The imaging of energetic neutral atoms (ENAs) has become an established means of remote sensing plasma distributions in planetary and space science (Wurz 2000). Recent examples include the study of Titan's exosphere (Mitchell et al. 2005), the terrestrial ionosphere and interplanetary medium by LENA (Moore et al. 2003), or the heliospheric ENAs by the *Solar and Heliospheric Observatory* (*SOHO*; Hilchenbach et al. 1998). An ENA starts as an ion, which is accelerated by an electromagnetic field until it exchanges its charge with a neutral atom of the ambient gas. It retains its original energy but is not influenced by electromagnetic fields anymore. It leaves the place of its birth on a ballistic trajectory and may reach regions far away from the original population of ions. Among many other applications, ENA imaging has been proposed (Gruntman et al. 2001; Fahr & Scherer 2004) and is planned to be used (McComas et al. 2004) to investigate the boundary of the heliosphere and the interstellar medium itself.

Heliospheric ENAs are predominantly hydrogen neutrals that have been produced on the far side of the termination shock in the inner heliosheath, where the solar wind has been slowed down to subsonic speed. There, ENAs are continually produced by charge exchange between interstellar neutrals and protons from the solar wind or from other ion populations. These processes ought to result in a detectable flux of inward-moving ENAs from the inner heliosheath (Gruntman et al. 2001; Fahr & Scherer 2004). Imaging these ENAs and their energy spectra would reduce our considerable uncertainties about the termination shock, the heliosheath surrounding it, and in general the interaction of the heliosphere with the local interstellar medium.

In this article we present and discuss energy spectra of ENAs measured by the ASPERA-3 instrument on board the *Mars Express* spacecraft (Barabash et al. 2004). The neutral particle detectors of the ASPERA-3 instrument were originally conceived to image ENA fluxes from Mars. But a preliminary evaluation showed in some cases a signal of energetic neutral hydrogen even though the neutral particle detector (NPD) sensors were pointed away from Mars, which prompted further research on these particular events. It meant, quite uncommon for a Mars research experiment, that we sampled all data for which Mars is well out of the NPD field of view. We present all those ENA measurements with a nonplanetary origin and discuss possible explanations. As we see below, a heliospheric origin of these ENA streams cannot be proved for certain, but it is the most plausible explanation.
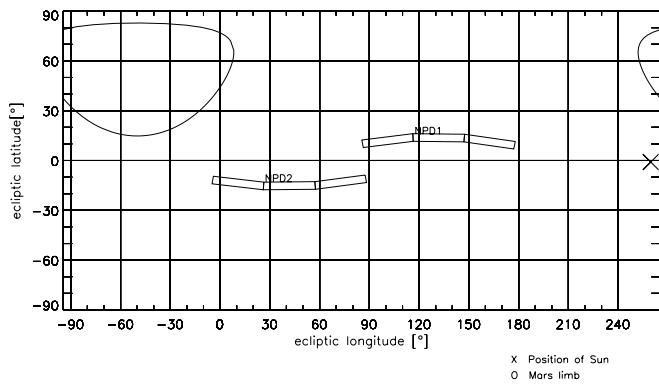
Fig. 1.—NPD observation conditions on 2004 February 24, 00:10 UT, in Mars orbit. The 2×3 elongated boxes are the fields of view of the two NPD sensors, each with their three angular channels ($5° \times 30°$ each). The positions of the Sun (*cross*) and the Mars limb are indicated as well.

2. INSTRUMENTATION

The ASPERA-3 instrument (Barabash et al. 2004) has been designed to study the interaction of the solar wind with the Martian atmosphere and to characterize the plasma and neutral gas environment in the vicinity of Mars. First results have been reported by Lundin et al. (2004).

The ASPERA-3 instrument comprises four different sensors. The ion mass analyzer and the electron spectrometer to measure local ion and electron densities, respectively, and the neutral particle detector (NPD) and the neutral particle imager (NPI) to detect ENAs. The results presented here are restricted to neutral particle measurements. Particular attention has been paid to those NPD data sets for which the field of view of the sensors is directed away from Mars.

The NPD consists of two identical sensors, NPD1 and NPD2, that are sensitive to ENAs in the energy range of 0.1–10 keV using the time-of-flight (TOF) technique. Each sensor has one start and three stop surfaces that provide an angular resolution of roughly $30°$ in azimuthal direction and $4°$ in elevation direction, which is shown in Figure 1.

The energy and the mass of an incident particle can be reconstructed from the TOF between start and stop surface and from the pulse height of the stop signal. Principally, this design enables us to distinguish oxygen from hydrogen in the Martian exosphere (Grigoriev et al. 2003).

3. DATABASE

The database for the search for ENA fluxes without planetary origin comprises all data sampled in RAW and in TOF operation mode of NPD (Barabash et al. 2004) for which a Martian origin can be excluded, i.e., Mars is outside the field of view of NPD. There are several time periods from 2003 July until 2005 March that are useful for this research topic. There also exists a so-called BINNING mode, but the TOF information is compressed into only 16 instead of 256 bins in this mode. The TOF information thus is not sufficient to obtain a reliable energy spectrum, and therefore BINNING mode data have been omitted from this analysis.

This database includes all data sets from the cruise phase and the few data sets from Mars orbit where the angle between the Mars limb and the closest edge of the field of view is larger than $45°$. All including, there are 10 different dates from the cruise phase and 102 dates from the Mars orbit that have been found to meet our criterion.

Figure 2 gives an overview of four arbitrarily chosen measurement locations in the ecliptic reference frame during cruise
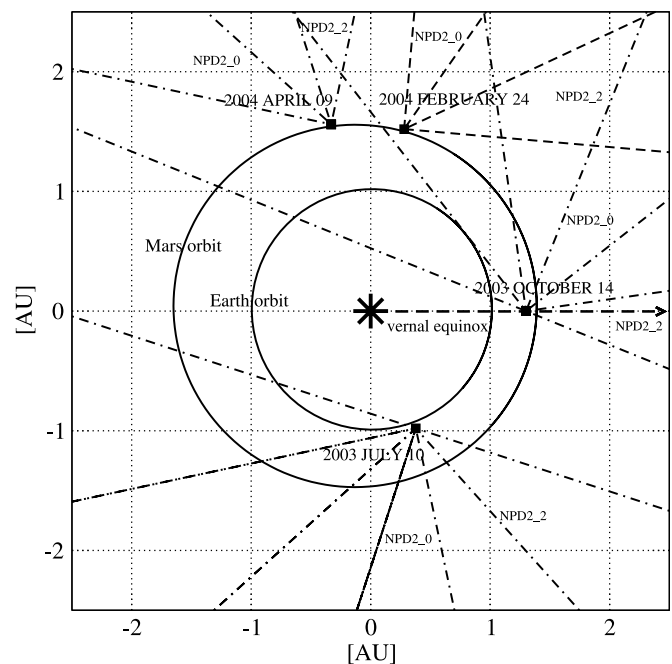
Fig. 2.—Overview of ENA observations, projected on the Earth ecliptic plane. Shown are four specific measurement locations between 2003 July and 2004 April. The Mars orbit insertion took place in 2003 December.

and orbit phase. The black ellipses are the Earth and Mars orbits, and the wedge-shaped sectors indicate the fields of view of the two NPD sensors for the indicated dates of observation.

4. SPECTRUM RECONSTRUCTION

The NPD sensor accumulates TOF information of incoming ENAs in steps of 1 s, but 10 minutes of integration time are generally required to obtain a TOF spectrum with reasonably small random fluctuations. This implies that we have discarded any short-scale time variations in our analysis. Figure 3 gives an example of a raw TOF spectrum (*top panel*) that has been converted into an energy spectrum (*bottom panel*). The value of each TOF bin corresponds to the average count rate per second.
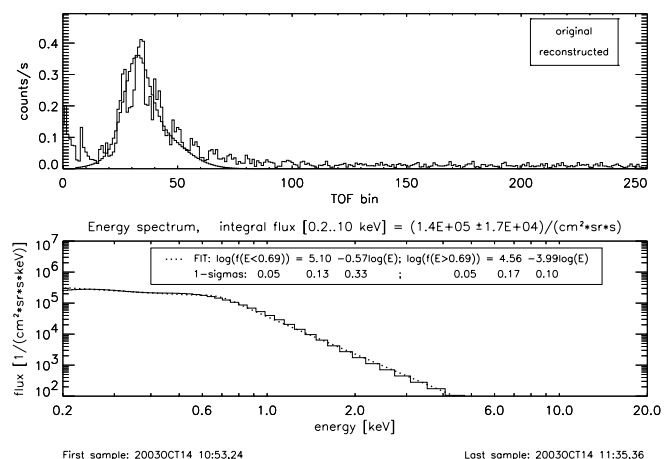
Fig. 3.—Example of a TOF spectrum for 2003 October 14, from NPD1, channel 0. Every incoming ENA is stored as a single count in one of the 256 TOF bins, each 8 ns wide. The top panel shows the original TOF spectrum (accumulated for 2000 s) and the reconstructed TOF signal after background removal and noise filtering. The bottom panel shows the energy spectrum calculated from the reconstructed TOF signal above and a fit to this spectrum (*dotted line*).

To convert the uncalibrated TOF spectrum into an energy spectrum in units of $cm^{-2}\ sr^{-1}\ s^{-1}\ keV^{-1}$ we assume that all detected ENAs are hydrogen atoms between 0.1 and 10 keV and that all six of the different microchannel plate detectors behave identically. Whereas the latter assumption is justified by laboratory calibration, the first assumption is only justified as long as we are dealing with nonplanetary ENAs. The Martian exosphere, by contrast, is bound to produce oxygen ENAs in abundance as well. The TOF signature of helium ENAs would hardly be discernible from hydrogen, but in interplanetary space the flux intensity of helium ENAs of about 1 keV will be orders of magnitude lower. A possible contribution by helium ENAs to the signals is therefore disregarded in the present analysis.

First, we subtract the noise background (see the Appendix for more information) caused by UV photons. If an ENA signal beyond the background is recognizable, we apply a low-pass filter (Marshall & Verdun 1990) to eliminate any short-period (shorter than 10 TOF bins) signal, including the harmonic noise caused by the sensor electronics (see, e.g., Fig. 3). We then invert the instrument response by searching for an optimal fit function, which, applied to the instrument response function, comes closest to the observed TOF spectrum using a least-squares method. Finally, to convert the count rates of the reconstructed TOF spectrum into differential fluxes, the count rates have to be divided by the product of the energy-dependent detection efficiency, geometrical factor, and the corresponding energy range of the TOF bin.

We retrieve from the reconstruction only four parameters that have been fitted to the energy spectrum between 0.2 and 10 keV: the slope at low energies (a_1), the slope at high energies (b_1), the place of the rollover (c), and the integral flux. In the subsequent discussion, the integral flux will be understood to cover the energy range from 0.2 to 10 keV unless specified otherwise. Although particles with energies between 0.1 and 0.2 keV are detected, we have chosen 0.2 keV as the lower cutoff, because the efficiency for energies between 0.1 and 0.2 keV is not well known. Integrating over this energy range would result in highly uncertain flux estimates (see the Appendix for further information). We find, within the range of uncertainty, that the vast majority of the resulting energy spectra can adequately be parameterized by a simple two-composite power law in the range between 0.2 and 10 keV, according to

$$f(E) = \begin{cases} a_0 E^{a_1} & \text{if } E < c, \\ b_0 E^{b_1} & \text{if } E \geq c. \end{cases} \tag{1}$$

5. OBSERVATIONS

The majority of TOF spectra in our database (a total of 205 spectra) of nonplanetary ENA streams show only noise, or they have an insufficient signal-to-noise ratio so that one cannot put any constraints on the reconstructed energy spectra. Our detection limit for ENA signals lies at $\sim 5 \times 10^3\ cm^{-2}\ sr^{-1}\ s^{-1}$. In the subsequent discussion we first give an overview of all 205 measurements before concentrating on the occasions where an ENA signal is clearly visible.

Figure 4 shows the integral fluxes as a function of observation date for all measurements from the database, including ill-defined spectra and measurements with no signal at all. Obviously, there are long observation gaps. During cruise phase the sensor was switched on only on a few occasions. After Mars orbit insertion the sensor was directed to Mars for most measurements, since the primary goal of ASPERA-3 was to study the Martian atmosphere. The fluxes seem to decrease with time and the vast majority of measurements from 2005 shows no signal at all with the exception
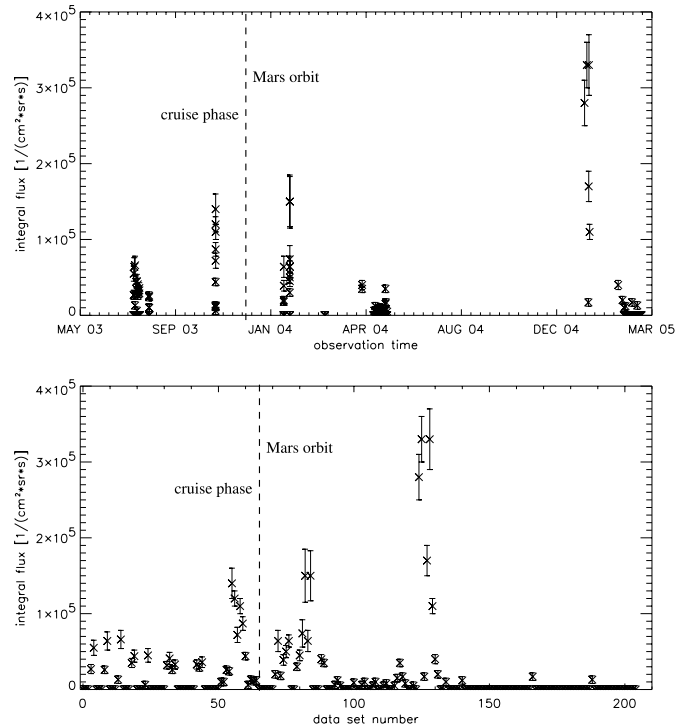
Fig. 4.—Integral flux vs. observation time for all measured spectra as a function of observation time (*top*) or as a function of data set number (*bottom*). The dashed line separates the observations obtained during cruise phase from those on Mars orbit. The second half of the data set (data set number 124–204) belongs to the short time interval 2005 February–March.

of the subset mentioned in § 5.2. Figure 4 shows that flux variations from the detection limit up to $10^5\ cm^{-2}\ sr^{-1}\ s^{-1}$ can occur on timescales of months. It is difficult to tell temporal from spatial variations with our sparse data set. Generally, the pointing direction of the field of view also changes from one observation opportunity to the next. Beside the long observation gaps, the spatial distribution of the observations is not favorable either. Virtually all useful data were measured when the field of view of the NPD was close to the ecliptic plane. After all, ASPERA-3 was designed as a Mars exploration experiment. It was not set up to search for nonplanetary ENA signals.

In short, the integral fluxes show big variations, but these are either stochastic or on timescales shorter than we can resolve with the few useful data sets.

5.1. *The Typical ENA Spectrum*

Figure 5 shows a typical example of an energy spectrum, reconstructed from NPD2 data measured on 2003 July 10 during the cruise phase. The signal is not of planetary origin since all planets are too far away and outside the field of view. It is a typical example insofar that from the 66 measurements having a sufficiently high signal-to-noise ratio, 51 result in energy spectra that are appropriately characterized by a two-composite power law with a moderate decrease at low energies, a rollover somewhere close to 0.8 keV, and a steeper decrease at higher energies.

If one displays the parameter for the rollover of all available 66 spectra on one single plot, one recognizes that a few data points lie far away from the typical value found in the early measurements during cruise phase. Figure 6 shows the position of the rollover, which is the best-defined parameter in the analysis. It can reasonably be defined even for the few cases in which the energy spectrum does not follow a two-composite power law but shows one single peak.
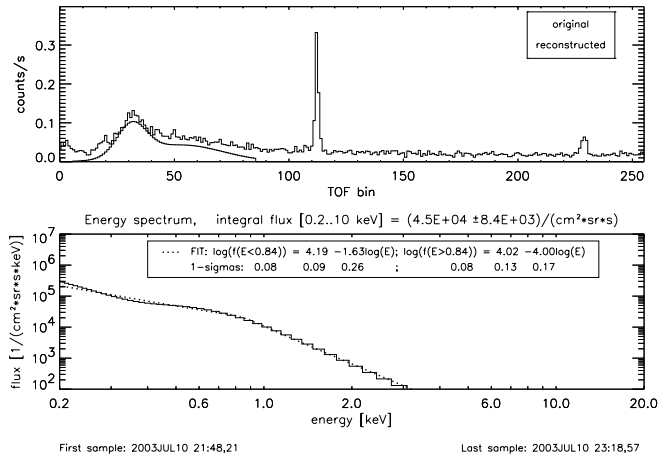
Fig. 5.—Typical example for a nonplanetary ENA signal, measured during cruise phase. The data format is the same as in Fig. 3. The top panel shows the TOF spectrum, averaged over 86 minutes of data; the narrow lines at TOF bin 112 and 229 are spikes introduced by the sensor electronics. They were removed from the TOF spectrum before further analysis.

5.2. *Outliers or Martian Contamination?*

Looking at Figure 6 we find that the data obtained during cruise phase show a consistent result. Afterward, the variation of the spectral parameters increases significantly. This may indicate an instrumental degradation, but it is more likely that Mars acts as a source of contamination once *Mars Express* is in orbit, although all data sets in which Mars gets close to the field of view have been excluded from our analysis.

From the 66 data sets displayed in Figure 6 we selected 51 spectra, which are displayed in Figure 7. All of them belong to the time span between 2003 July and 2004 May. Among the numerous measurements from 2005 January to March only eight show a recognizable ENA signal. However, the corresponding energy distribution of these fluxes does not fit the typical spectrum (see Fig. 5 for details). It shows a peak between 1 and 1.3 keV that is similar to spectra obtained from the Mars limb observation (see Fig. 8). Therefore, these measurements are excluded from further discussion. Another reason to disregard these eight events is the fact that all of them are measured with the field of view coaligned to the Parker angle of the interplanetary magnetic field. A solar wind-induced signal is therefore plausible for this sub-data set, contrary to the majority of nonplanetary signals discussed in § 5.3.

5.3. *Statistics of Nonplanetary ENA Signals*

In the following discussion we exclude the eight events in 2005 from the evaluation, as well as the other few events with a
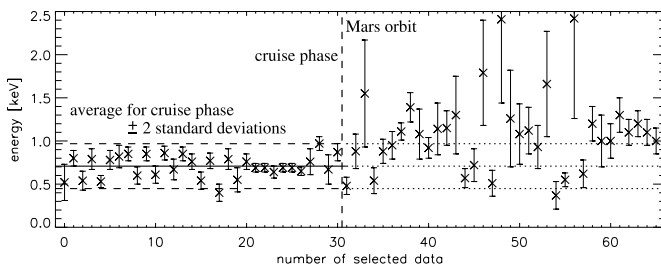
Fig. 6.—Position of rollover of all available 66 spectra. Large error bars belong to measurements with a poor signal-to-noise ratio. The last eight events (numbers 58–65) with an untypically high rollover between 1 and 1.5 keV, all of them measured in 2005, probably have been produced by a different process.
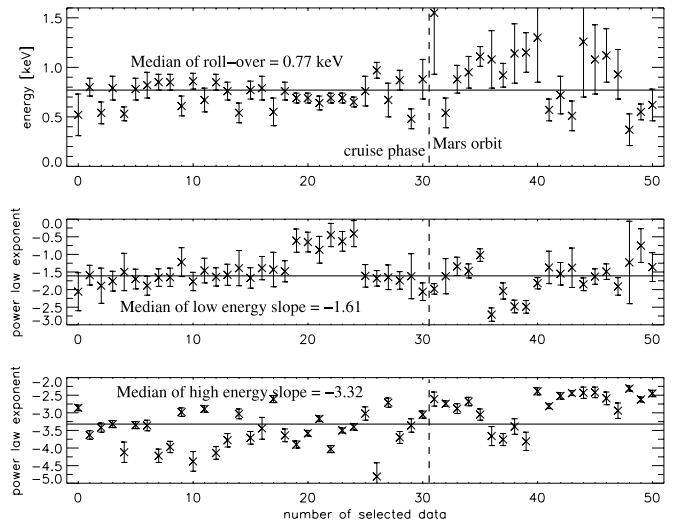
Fig. 7.—Median values of rollover (*top*), low-energy slope (*middle*), and of high-energy slope (*bottom*) for all spectra that can be appropriately characterized by a two-composite power law.

spectral shape that cannot be characterized by a two-composite power law and a poor signal-to-noise ratio. This leaves us with 51 spectra that seem to belong to one single spectrum class. The spectral parameters of the remaining data sets are shown in Figure 7, together with the median values. The spectrum shape is described by

$$f(E) = \begin{cases} a_0 E^{-1.6} & \text{for } E < 0.77 \text{ keV}, \\ b_0 E^{-3.3} & \text{for } E \geq 0.77 \text{ keV}, \end{cases} \qquad (2)$$
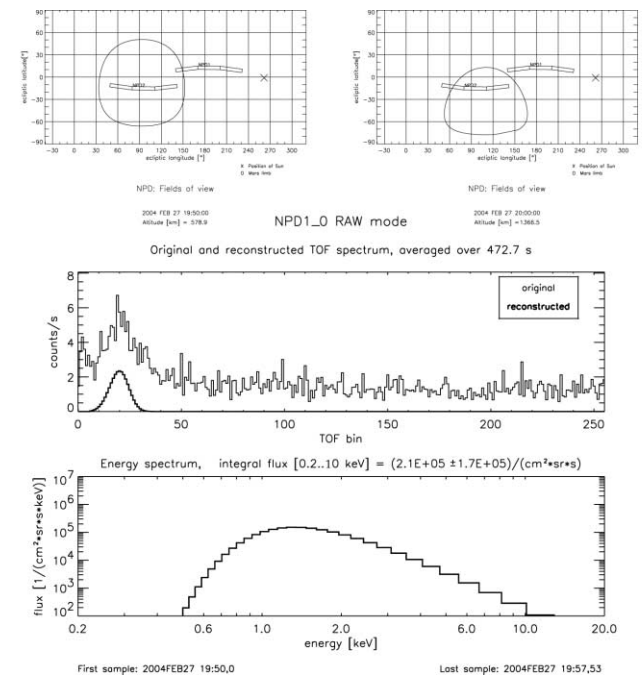
Fig. 8.—Solar wind interacting with the Martian atmosphere. The two panels at the top show the observation setting on the evening of 2004 February 27; the two bottom panels show the ENAs detected from direction NPD1_0 during the observation period of 8 minutes. Since the edge of the NPD1 field of view is near the Mars limb, a distinct peak in the TOF spectrum is detected. The resulting spectrum is typical for solar wind protons that have been neutralized in the upper parts of the Martian atmosphere (see Futaana et al. [2006] for further information). It is not typical for the 51 ENA events plotted in Fig. 7.
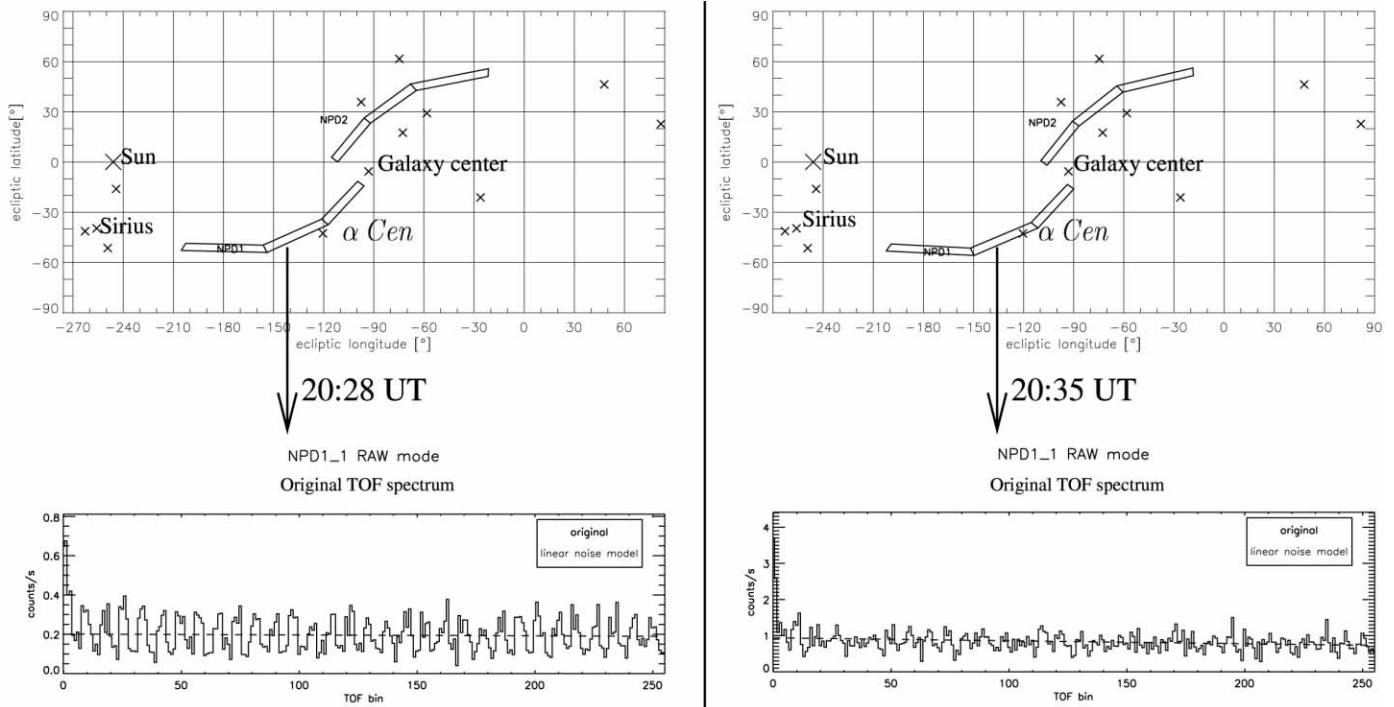
Fig. 9.—UV response of the NPD sensor. The field of view and the position of the brightest stars for the measurement on the evening of 2003 July 13 are shown in the top panels. On direction NPD1_1 the UV flux from α Cen raises the noise level by a factor of 5 in the TOF spectra (see the bottom panels). But no TOF signal whatsoever can be seen above this background.

where the statistical $1\,\sigma$ error bars of the average values for the data in Figure 7 are in the range $-2.1 < a_1 < -1.1$, 0.55 keV $< c < 1.0$ keV, and $-3.9 < b_1 < -2.7$, and a_1, b_1, and c are defined in equation (1).

6. DISCUSSION

Let us shortly discuss possible explanations for the ENA signal presented in the previous section. Some explanations can be ruled out; for others we may never be able to reach a definitive conclusion with the available database.

6.1. Comparison to Martian ENA Spectra

There is a general difference between the typical nonplanetary spectrum shown in Figure 5 and signals of Martian ENAs. The latter often show energy spectra with a distinct peak or a rollover at high energies well above 1 keV, whereas the well-defined spectra of nonplanetary ENA events share a rollover between 0.7 and 0.9 keV. We find that the integral fluxes of ENAs produced by interactions with the Mars atmosphere may reach several 10^6 cm^{-2} sr^{-1} s^{-1}, which is an order of magnitude higher than the highest flux measured in the case of nonplanetary ENA signals (see Fig. 4).

Figure 8 illustrates one of many occasions where the field of view has approached the Mars limb and a stream of ENAs is detected that obviously originate from Mars. This is the reason why any signal measured when the field of view was closer to the Martian limb than $45°$ has been excluded from our study in the first place. In the case of Figure 8, the energy spectrum with a distinct peak at 1 keV hints to solar wind protons that have been neutralized in the Martian atmosphere (Futaana et al. 2006). Such a signal can be easily told from nonplanetary spectra as listed in Figure 7. It has, however, a certain similarity to the ENA

signals in 2005 with an untypically high rollover (see § 5.2), which after all might reflect a Martian contamination as well.

6.2. UV Sensitivity

Stars produce high fluxes of UV photons that might—by interaction with the start and stop surfaces of the NPD detector—give us a mock signal. The Sun is in all measurements outside the field of view, but we needed to check if single stars or the galaxy as a whole could be the source of the unexplained neutral streams.

This question is answered by the measurement on 2003 July 13. By a stroke of luck α Cen, the closest star to our Sun, wandered across the field of view of the NPD1 detector. Figure 9 shows the field of view and the position of the brightest stars at two different times during the observation period; below are the registered count rates and the average TOF spectra. As a matter of fact, UV photons cause the noise floor in the TOF spectra, and passing nearby stars raise this floor by factors of 4–5, but they do not produce a peak in the TOF spectrum that could be mistaken for an ENA signal.

In summary, not one of the 51 events mentioned in § 5.3 can be related to a nearby star. Stellar UV light does not produce a TOF spectrum that could be mistaken with signals such as those shown in Figure 5. The global spatial pattern of the integral fluxes (see Fig. 12 in § 6.4) is not consistent with nearby stars or the galactic center as source regions of the signals.

6.3. Suprathermal Ions and Parker Angle

There is—in addition to the anomalous energy spectrum—another reason to separate the eight events (see § 5.2) in 2005 from the typical ENA measurements. They are aligned with the direction of the magnetic field of the solar wind. Most other signals, those measured during cruise phase in particular, show
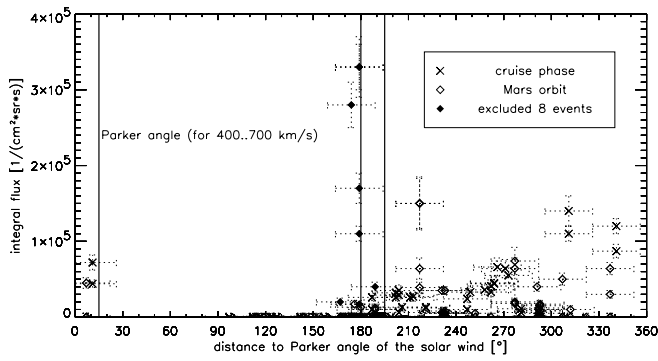
FIG. 10.—ENA flux vs. pointing directions of NPD sensor for all measurements. The vertical lines indicate the range of Parker angles for varying velocities of the solar wind. The eight data points from 2005 (*filled diamonds*), for example, lie close to the direction of particles that would follow the solar wind magnetic field coming from the antisunward hemisphere. The interval at 0° indicates the sunward direction of the magnetic field. Data obtained during cruise phase (*crosses*), Mars orbit in 2004 (*diamonds*), and Mars orbit in 2005 (*filled diamonds*) have been distinguished, since the data from the cruise phase are the most reliable ones.

FIG. 11.—Results of a SRIM simulation with 100 keV protons backscattering on the NPD start surface. The top panel shows the energy distribution of those backscattered protons that reach the stop surface. The middle panel shows the TOF spectrum NPD would measure for such a particle source. The bottom panel shows the reconstructed energy spectrum.

no correlation with the direction of the Parker angle at the given heliocentric distance. This is illustrated by Figure 10.

For those events for which the NPD aperture actually is co-aligned with the interplanetary magnetic field, suprathermal ions of 100 keV seem to be a possible explanation. Energetic ions created at a distant shock travel along the magnetic field lines and enter the NPD instrument. These ions are too energetic to be eliminated by the electric field for ion suppression in the collimator, which sweeps away all ions below 70 keV. The energetic ions then hit the start surface and produce secondary particles that could be mistaken for ENAs hitting the stop surfaces. However, simulations with the SRIM software (Ziegler et al. 1996) lead us to conclude that such so-called suprathermal protons of 100 keV are no reasonable explanation for our signals. It would take a flux of 10^5–10^6 cm^{-2} sr^{-1} s^{-1} of suprathermal ions to mock an ENA signal of 10^4 cm^{-2} sr^{-1} s^{-1}. Moreover, Figure 11 shows that neither the TOF nor the energy spectrum of the backscattered ions gets close to the typical nonplanetary ENA signal (cf., e.g., Fig. 5).

6.4. *A Spatial Pattern*

There is one remarkable correlation that cannot be explained by an observational bias. The ENA signals show a geographic pattern, with a preferred direction lying between 30° and 90° ecliptic longitude. The correlation of integral flux with ecliptic longitude is statistically significant at the 95% confidence level for a Spearman rank correlation test applied to 12 data bins of 30° each (Fig. 12, *bottom panel*). This is true whether we restrict the analysis to the well-defined 51 spectra or include all 205 measurements.

Figure 12 shows the variation of integral flux with ecliptic longitude. The Sun is moving compared to the local interstellar
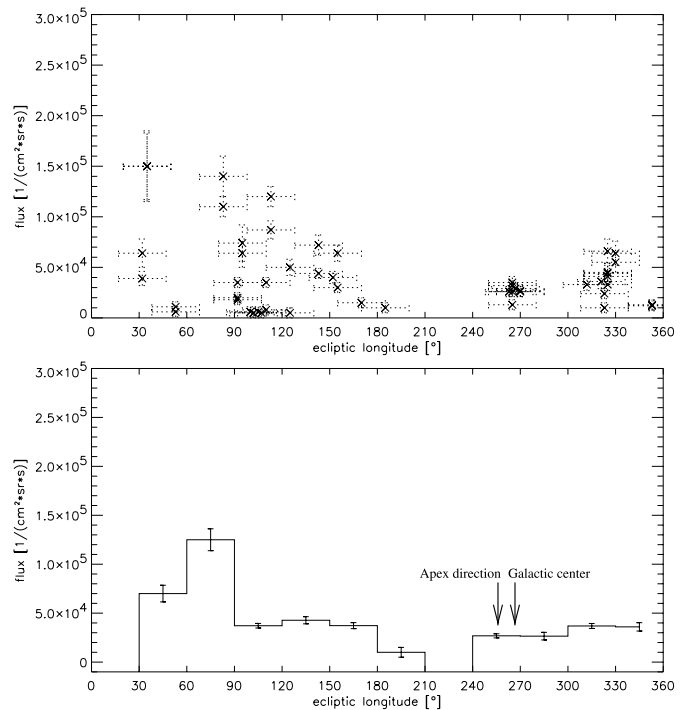
FIG. 12.—Integral ENA flux vs. direction of origin. Shown are all measurements whose spectral shape fits to the class described in § 5.3. The arrows at 255° and 267° ecliptic longitude denote the arrival direction of the interstellar neutral flow and the direction toward the galactic center. The bottom panel shows the data from the top panel, redistributed into 12 bins.

medium toward 255° with about 25 km s^{-1}. This results in a stream of low energetic hydrogen and helium neutrals flowing from this direction toward the Sun (Witte et al. 2004; Lallement et al. 2005). The ENA signal measured by ASPERA-3, on the other hand, seems to increase in integral flux between 30° and 90°, around the anti-apex direction, while a zone with scarcely any signal expands from 180° to 300°. It is deplorable that so few measurements fall within the region of 0°–90° ecliptic longitude where the highest fluxes seem to originate from. Nothing can be said about the latitudinal distribution of the signals, as the NPD detector was aligned to the ecliptic plane in virtually all instances.

It may be worth considering that Hilchenbach et al. (1998) have published results of energetic hydrogen measurements performed by the Highly Suprathermal Time-Of-Flight (HSTOF) sensor on the *SOHO* mission. Their instrument had a different energy range (55–80 keV) compared to ASPERA-3. But, consistent with our findings (Fig. 12), they also observed a preferred direction of origin for their ENA signal between 70° and 90° ecliptic longitude. The reported integral fluxes (Czechowski et al. 2005) fall within the same order of magnitude as the ENA measurements presented in this work if one assumes a power-law decrease between 6 and 60 keV according to $f(E) \sim E^{-3.5}$. Until now, the process that produces the ENA signals reported by Hilchenbach et al. (1998) is not identified with certainty. The spatial and temporal resolution makes it hard to decide between a local, interplanetary (Kotá et al. 2001), or remote heliospheric origin of the ENAs (Czechowski et al. 2001, 2005).

7. CONCLUSION

We have detected signals of energetic neutral hydrogen over a time range of 10 months. For the statistical evaluation we have accounted for all data sets for which Mars is well out of the field of view, be there a recognizable signal or not. Fifty-one of the 66 energy spectra with a favorable signal-to-noise ratio fit into one single spectrum class

$$f(E) = \begin{cases} a_0 E^{-1.6} & \text{for } E < 0.77 \text{ keV}, \\ b_0 E^{-3.3} & \text{for } E \geq 0.77 \text{ keV}, \end{cases} \quad (3)$$

independent of observation date or pointing direction. The integral flux between 0.2 and 10 keV varies from 5×10^3 up to 10^5 cm^{-2} sr^{-1} s^{-1} either spatially or on small timescales that we cannot resolve. These signals do not correlate with the position of Earth, Mars, Jupiter, or Saturn and their spectra look different from typical ENA signals from Mars.

The source of the ENA signal is not identified with confidence yet. There has to be a mechanism that produces neutral hydrogen fluxes on the order of 10^4–10^5 cm^{-2} sr^{-1} s^{-1} with velocities around 400 km s^{-1}. These velocities are an order of magnitude higher than the relative motion of the Sun through the local interstellar cloud, and the direction where we measure the highest fluxes of ENA atoms lies between 90° and 180° away from the direction of the interstellar neutral flow and from the galactic center.

Based on our present analysis, our conjecture is that we are observing energetic neutral particles that were produced in the area of the heliospheric termination shock. The typical integral flux of several 10^4 cm^{-2} sr^{-1} s^{-1} is about an order of magnitude higher than fluxes derived from theoretical models (Fahr & Scherer 2004; Gruntman et al. 2001) but is consistent with ENA measurements done by HSTOF on *SOHO* (Czechowski et al. 2005).

The main objection to the heliospheric explanation is the temporal variation of the integral fluxes for the same region (see

Fig. 12, *top panel*). Generally, the distance to the source region of the ENA signal could be estimated if we could determine the timescale of flux variations. A heliospheric origin of the observed ENAs requires this timescale to be longer than a few months, since an ENA of energy 0.3 keV takes about 2 years to travel the distance of 100 AU from the termination shock to the inner solar system, whereas a 2 keV ENA takes only 9 months. Therefore, even an ENA event that is a short pulse at the termination shock will be spread out in time during its propagation to the detector over many months. If the signal is found to vary over a timescale of one month or less, the ENA signal has to originate from a localized source within a few AU distance, and processes in the local solar wind, such as CIRs, would be needed to explain our observations. Unfortunately, there are only two occasions where we observe the same direction more than once within 1 month. The first one are the dozen measurements between 320° and 335° ecliptic longitude in Figure 12 that have been measured during 2003 July in cruise phase. The spectrum remains the same but the integral flux dropped from 6.6×10^4 to 1.0×10^4 cm^{-2} sr^{-1} s^{-1}. But since these were the very first measurements, this drop in count rates might also be explained by a water contamination of the active detector surface, which was slowly lost during the first measurements. The only two occasions for which a flux below 3×10^4 cm^{-2} sr^{-1} s^{-1} was measured, the integration times were only 15 minutes compared to typically 1 hr for the other data in 2003 July. In any case the timescale of the ENA variations must be longer than days since there was a measurable signal from this direction whenever the detector was operational in July. As far as cruise phase data are concerned, there is no overlapping between regions where a signal was detected and regions where no signal was detected from 2003 July to October. The other region that we observe more than once within a month is the one between 30° and 40° ecliptic longitude. It was covered twice, namely, on 2004 January 5 and January 12. The integral flux increased by a factor of 2.5 within a week. However, in this time span *Mars Express* approached Mars from 11 to 4 Mars radii, and a Martian contamination once more cannot be excluded.

The temporal variability seems easier to be reconciled with a localized solar wind origin, but there are at least two objections against this explanation. First, a solar wind source is inconsistent with the observed direction of origin (see Fig. 12). Even if there are energetic protons produced in the vicinity of the NPD detector, for instance due to CIRs, they still need neutral hydrogen atoms to charge exchange in order to be detected as ENAs. Since the interplanetary hydrogen density is higher toward the apex direction of the heliosphere, a localized ENA source would not preferentially be observed from downwind direction. Second, the ENA signal is at least 3 orders of magnitude higher than one would expect if it were caused by protons that have been accelerated in a nearby CIR. The differential flux of ENAs at 1 keV energy that can be locally produced calculates to

$$j_{\text{ENA}} = \sigma \int_{\text{LOS}} (n_{\text{H}} \, j_P) \, dl, \quad (4)$$

where j_P is the differential flux intensity of 1 keV protons in units of cm^{-2} sr^{-1} s^{-1} keV^{-1}, $\sigma = 2 \times 10^{-15}$ cm^2 is the cross section for the charge exchange between a 1 keV proton and a thermal hydrogen atom (Gruntman et al. 2001), $n_{\text{H}} = 0.1$ cm^{-3} is the interplanetary hydrogen particle density, and the integral is a line-of-sight integral taken over a typical length scale. For a local source in the inner solar system we set $\int_{\text{LOS}} dl = 1$ AU.

Equation (4) then yields as a rough estimate for the required proton flux

$$j_{\mathrm{ENA}} = 10^{-3} j_P. \qquad (5)$$

Since we typically observe at 1 keV $j_{\mathrm{ENA}} = 10^4$ cm^{-2} sr^{-1} s^{-1} keV^{-1}, it would require at least (eq. [5]) a differential flux of $j_P = 10^7$ cm^{-2} sr^{-1} s^{-1} keV^{-1} 1 keV protons to reproduce our ENA observations. This gets close to the flux intensity of the solar wind itself, while we are looking away from the Sun! Spectra of high-energy protons from CIR events are available; see, for instance, Desai et al. (1999) for the energy range between 50 keV and 20 MeV. But to our knowledge the energy spectrum of CIR-protons at 1 keV has not been measured yet. If we extrapolate the value at 100 keV found by Desai et al. (1999) down to 1 keV assuming a power law with an exponent of -2 (which seems to be the most extreme case according to Figs. 4 and 6 in

Desai et al. 1999), we find only $j_P = 10^4$ cm^{-2} sr^{-1} s^{-1} keV^{-1} at 1 keV. This is 3 orders of magnitude too low.

We have checked that an instrumental effect, such as high-energy protons scattering on the start surface, cannot explain the measurements. The Sun is always outside the field of view, and the observed ENA signal shows no correlation with the Parker angle of the solar wind. We also have shown that the signal is not caused by UV photons; the geographical pattern of the signals does not correlate with bright nearby stars or with the galactic center.

It is unclear whether ASPERA-3 will sample many more data sets that can be used for the study presented here, since most of the well-defined spectra have been sampled in 2003 during the cruise phase. For the upcoming *Venus Express* mission it would be favorable to sample more data during the cruise phase and to cover the entire sky. Further insight into ENAs of nonplanetary origin will hopefully be provided by NASA's *Interstellar Boundary Explorer* (*IBEX*) mission (McComas et al. 2004).

APPENDIX

The estimate of the noise level has a big influence on the resulting energy spectrum. We have verified with numerical simulations of the instrument response that UV photons are the prime source of background in the TOF spectra. The UV photons originate from resonant backscattering in interplanetary hydrogen (Lyα emission lines account for 600 Ra) and helium (only 7 Ra); bright nearby stars and the galactic disk increase the UV flux to several 1000 Ra.

The count rates registered in the higher TOF bins from 100 to 256 can be understood as result of a start and a stop signal of two different, uncorrelated photons that have been registered by the sensor almost simultaneously. We also know from calibration that the counter surfaces are insensitive to ENAs below 0.1 keV. Therefore, we use a linear noise model whose parameters are fitted to the count rates in the highest TOF bins from 200 to 256. After subtracting the background, all the bins that correspond to energies below 0.1 keV will be excluded from the analysis, as will be the lowest few TOF bins.

The range of uncertainty is calculated for each bin through the entire reconstruction analysis. The prime sources of error are the counting statistics themselves, the uncertainty in estimating the UV background and the poorly known detection efficiency for atoms at energies below 0.3 keV.

Figure 13 gives an extreme example but also illustrates the solution: Since the error bars for a single energy bin are large, it is intuitive to characterize the reconstructed energy spectrum by only a few parameters, which are much better constrained than the values of a single energy bin. The relative uncertainty of the derived parameters amounts to roughly 10% only, which is also shown in Figure 13. Below 0.3 keV the uncertainty of the NPD detection efficiency becomes troublesome, whereas at high energies poor counting statistics is the prime source of uncertainty. The effect of these errors is comparable to the intrinsic energy resolution limit (FWHM criterion applied to the resulting peak for a monoenergetic beam) $\Delta E/E \approx 0.3$ between 0.3 and 1 keV.

Thus, instead of 256 different energy bin values, each of them with considerable uncertainty, we retrieve from the reconstruction only the four parameters mentioned in § 4.
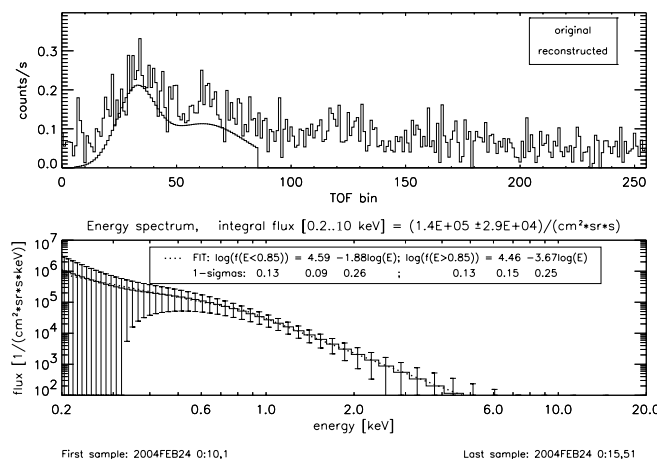
FIG. 13.—Uncertainty range of single energy bins (*bottom*) for a measured TOF signal (*top*). The data format is the same as in Fig. 3, but for 2004 February 24. Note that the individual error bars may be larger than the bin values themselves.

REFERENCES

Barabash, S., et al. 2004, in *Mars Express*: The Scientific Payload, ed. A. Wilson (Noordwijk: ESA), 121

Czechowski, A., Hilchenbach, M., & Hsieh, K. C. 2005, A&A, 431, 1061

Czechowski, A., et al. 2001, A&A, 368, 622

Desai, M. I., et al. 1999, J. Geophys. Res., 104, 6705

Fahr, H.-J., & Scherer, K. 2004, Ap&SS Trans., 1, 3

Futaana, Y., et al. 2006, Icarus, in press

Grigoriev, A., Barabash, S., & Fedorov, A. 2003, ASPERA-3/NPD2 FM2 Calibration Rep., http://aspera-3.irf.se

Gruntman, M., Roelof, E. C., Mitchell, D. G., Fahr, H.-J., Funsten, H. O., McComas, D. J. 2001, J. Geophys. Res., 106, 15767

Hilchenbach, M., et al. 1998, ApJ, 503, 916

Kotá, J., Hsieh, K. C., Jokipii, J. R., Czechowski, A., & Hilchenbach, M. 2001, J. Geophys. Res., 106, 24907

Lallement, R., Quémerais, E., Bertaux, J. L., Ferron, S., Koutroumpa, D., & Pellinen, R. 2005, Science, 307, 1447

Lundin, R., et al. 2004, Science, 305, 1933

Marshall, A. G., & Verdun, F. R. 1990, Fourier Transforms in NMR, Optical, and Mass Spectrometry: A User's Handbook (Amsterdam: Elsevier)

McComas, D. J., et al. 2004, in AIP Conf. Proc. 719, Physics of the Outer Heliosphere, ed. V. Florinski, N. V. Pogorelov, & G. P. Zank (New York: AIP), 162

Mitchell, D. G., Brandt, P. C., Roelof, E. C., Dandouras, J., Krimigis, S. M., & Mauk, B. H. 2005, Science, 308, 989

Moore, T. E., et al. 2003, Space Sci. Rev., 109, 351

Witte, M., Banaszkiewicz, M., Rosenbauer, H., McMullin, D. 2004, Adv. Space Rev., 34, 61

Wurz, P. 2000, in The Outer Heliosphere: Beyond the Planets, ed. K. Scherer et al. (Katlenburg-Lindau: Copernicus), 251

Ziegler, J. F., Biersack, J. P., & Littmark, U. 1996, The Stopping and Range of Ions in Solids (New York: Pergamon)